

Extreme-point Symmetric Mode Decomposition-based Energy Integral Model for Bridge Abnormality Detection Using Ground-based Synthetic Aperture Radar

Songxue Zhao, Xianglei Liu,* and Runjie Wang

Key Laboratory for Urban Geomatics of National Administration of Surveying, Mapping and Geoinformation, Beijing University of Civil Engineering and Architecture, 1 Zhanlanguan Road, Beijing 100048, China

(Received April 2, 2023; accepted July 4, 2023)

Keywords: GB-SAR, bridge, abnormality detection, ESMD, energy integral

Ground-based synthetic aperture radar (GB-SAR), as a noncontact measurement technology, is widely used in the dynamic deflection monitoring of various bridges. Energy analysis is a popularized time–frequency domain technique for bridge abnormality detection. To improve the accuracy of bridge abnormality detection using GB-SAR, in this paper, we propose an extreme-point symmetric mode decomposition (ESMD)-based energy integral model based on the total energy function to identify the position and trend of bridge changes. First, ESMD with the wavelet synchro-squeezing transform (ESMD-WSST) high-frequency denoising processes are applied to reduce the effect of noise contained in the monitored dynamic deflection. Second, ESMD decomposition and instantaneous frequency calculation are performed on the denoised signal to obtain the integration time adaptively. Third, the instantaneous total energy of all reflection points on the lower surface of the bridge is calculated through the kinetic energy formula to improve the accuracy. Finally, instantaneous total energy integration is applied for energy accumulation calculation to accurately detect bridge abnormality without empirical judgment. The performance of the proposed model is verified through an on-site experiment of the Beishatan Bridge and comparing its result with that of the 3D laser model in the same period. The experimental results show that the proposed model can achieve high-precision identification of bridge abnormality positions and trends.

1. Introduction

Bridge dynamic deflection is one of the most important indicators to reflect the abnormality of a bridge structure.⁽¹⁾ Through the analysis of the dynamic deflection, the operating state of a bridge can be clearly known.⁽²⁾ Compared with traditional contact sensors, ground-based synthetic aperture radar (GB-SAR), as a noncontact measurement technology, can obtain the dynamic deflection of bridges in all types of weather and in a wide range of scales.⁽³⁾

At present, the time–frequency domain analysis (TFA) method is commonly used in the identification of bridge abnormality.⁽⁴⁾ TFA provides the joint distribution information in both

*Corresponding author: e-mail: liuxianglei@bucea.edu.cn
<https://doi.org/10.18494/SAM4413>

time and frequency domains. Moreover, it can clearly describe the relationship between the dynamic deflection frequency and time.⁽⁵⁾ TFA was first introduced together with the Fourier transform (FT).⁽⁶⁾ Through FT, the frequency information of the dynamic deflection can be obtained. However, FT has insufficient processing ability for nonstationary signals, and the moment when the frequency components appear cannot be known.⁽⁷⁾ The short-time Fourier transform (STFT) was later proposed to improve this deficiency to a certain extent.⁽⁸⁾ STFT multiplies the signal and the window function and then performs a one-dimensional FT. A series of FT results are obtained by sliding the window function, and these results are arranged to obtain a two-dimensional representation. However, the STFT window function is fixed, which cannot meet the frequency requirements of unsteady signal changes.⁽⁹⁾ Wavelet transform (WT) inherits and develops the idea of STFT localization.⁽¹⁰⁾ WT overcomes the disadvantage that the window size cannot change with frequency. Since the selected wavelet basis function will run through the whole wavelet transform analysis, WT does not have the characteristics of self-adaptation.⁽¹¹⁾ The Hilbert–Huang transform (HHT) has good adaptability, and its further step of empirical mode decomposition (EMD) decomposes signals on the basis of the time scale characteristics of the signal itself without presetting any basis functions.⁽¹²⁾ However, the EMD method has the problems of edge effects and mode mixing in signal decomposition.⁽¹³⁾ Compared with the EMD method, extreme-point symmetric mode decomposition (ESMD) adopts the internal extremum symmetrical interpolation to form the signal envelope, which reduces the effect of the uncertainty from the low-frequency component interpolation line.⁽¹⁴⁾ The ESMD method improves the linear interpolation method, increases the stability of the decomposition, and improves the phenomenon of excessively steep boundaries.⁽¹⁵⁾ At the same time, ESMD adopts the direct interpolation method for spectrum analysis, which can not only directly reflect the time-varying amplitude and frequency of each mode, but also clearly determine the instantaneous energy change.^(14–16)

Energy analysis is a common method for structural variation identification. Projecting structural energy changes based on the TFA method can identify the exact location and degree of structural variation. Yang *et al.* proposed a damage identification method based on the Hilbert spectrum to identify the multi-degrees-of-freedom linear system through the natural vibration signal of the structure and determine the structural damage.⁽¹⁷⁾ Roveri and Carcaterra used the HHT method to analyze the damage of bridge structures under dynamic loads without prior information and obtained the damage location through the peak information of the first instantaneous frequency.⁽¹⁸⁾ However, these methods achieve energy discrimination by approximately projecting the instantaneous energy on several fixed frequency bands of tiny windows. In this situation, there will be a large difference in the moment determination of energy mutation. Wang and Fang gave up using the spectrum method to represent the energy change of the signal and used the total kinetic energy formula to define the time-varying characteristics of energy using the ESMD method.⁽¹⁶⁾ The feasibility of the ESMD method was proved by a test experiment on the vibration signal of the wind field. Liu *et al.* used the ESMD method to decompose the response signal of the gradually collapsing building model into a series of intrinsic mode functions (IMFs) and performed a stability analysis on the instantaneous frequency and instantaneous total energy of each IMF.⁽¹⁹⁾ The experimental results showed that

the ESMD method can effectively analyze the building model stability. However, the ESMD method relies on empirical judgment for the identification of energy functions and lacks a clear indicator of quantitative structural abnormality.

To provide quantitative monitoring results for bridge abnormality, in this paper, we propose an ESMD-based energy integral model based on the total energy function to identify the position and trend of bridge changes. By integrating the instantaneous total energy, the energy accumulation of the reflection point on the lower surface of a bridge in a specific time window will be obtained to accurately judge the position of the bridge change. On the basis of the size of the energy integral, the bridge damage trend can be further judged.

2. Methodology

The overall workflow of the ESMD-based energy integral model proposed in this study is shown in Fig. 1. The key steps are as follows. First, ESMD with the wavelet synchro-squeezing transform (ESMD-WSST) high-frequency denoising is performed on the dynamic deflection collected by GB-SAR to obtain the denoised dynamic deflection signal as the original input signal.⁽²⁰⁾ Second, the instantaneous frequency of the input signal is calculated by ESMD decomposition, and the integration window t is defined in accordance with the frequency mutation interval. Third, the total kinetic energy formula is used to calculate the instantaneous total energy function $E(t)$ of the input signal, and then it will be integrated with the time window t to obtain the energy accumulation value EI . Finally, through the position of the reflection point

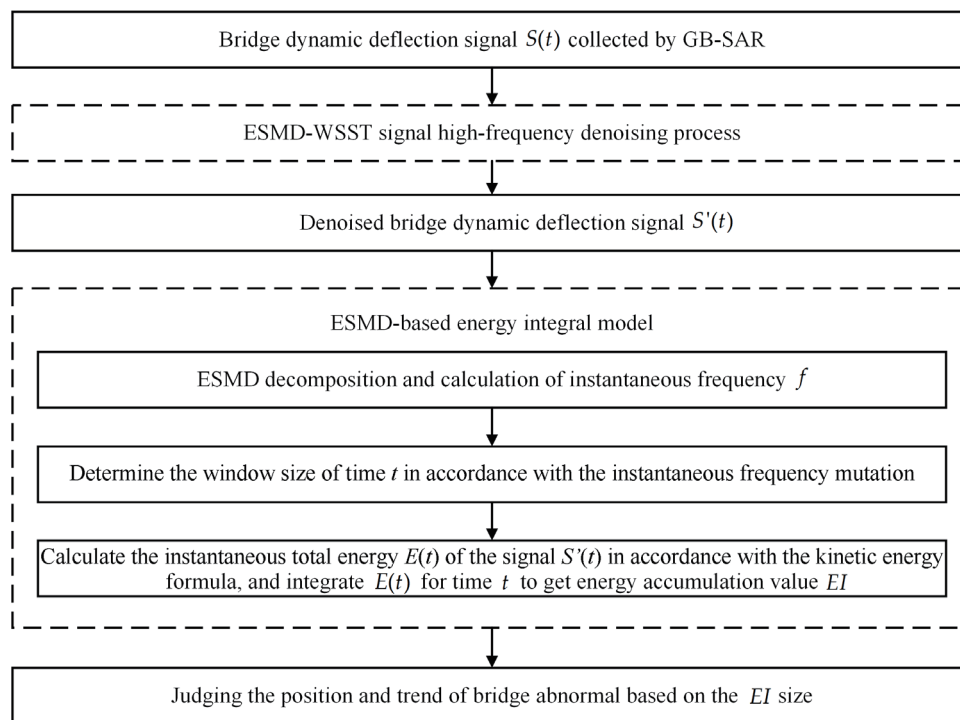


Fig. 1. Overall workflow of ESMD-based energy integral model.

corresponding to the absolute maximum value (relative maximum value) of EI , the position and degree of the bridge variation area can be judged.

2.1 Relationship between bridge abnormality and energy accumulation

Cracks are the main form of bridge abnormality. The cracks generated in a bridge structure will change the cross section of the dynamic deflection signal propagation. As air exists in a crack and the transmission coefficient of the vibration signal in the air is almost zero, the dynamic deflection will be diffracted after encountering the crack.

It is assumed that the dynamic load of a vehicle is transmitted in the form of a spherical wave. The wave will be reflected due to the obstruction of the boundary of the component during the propagation process. In practice, because of the modal change of the wave during reflection and the energy loss caused by the reflection interface, the energy of the reflected wave transmitted by the dynamic deflection to the position of the damping member is much smaller than that of the direct wave. In this situation, the vibrations received by the bridge damping member can be treated as direct waves.

When there are no cracks in the bridge components, the vibration received by the damping member can be considered as the part between the two wave lines with the angle θ_1 shown in Fig. 2. At a certain moment in the dynamic loading process, we assume that the total energy of the vibration caused by a vehicle is E . Then when only geometrical diffusion is considered, the energy of the direct wave received at the damper E_1 can be expressed as

$$E_1 = \frac{\theta_1}{2\pi} E. \quad (1)$$

We assume l_{s_1} as the wavefront length from the vehicle contact point to the damper inside the bridge. E_1 is the energy of the wave line l_{s_1} . Then, its energy per unit length ΔE_1 is

$$\Delta E_1 = \frac{\theta_1}{2\pi} E / l_{s_1}. \quad (2)$$

As shown in Fig. 3, when cracks appear in the bridge, it is assumed that the propagation of the wave is not affected by the cracks and still propagates in a straight line. Since the angle between the original direct wave lines is reduced to θ_2 , the received direct wave energy E_2 at this time is

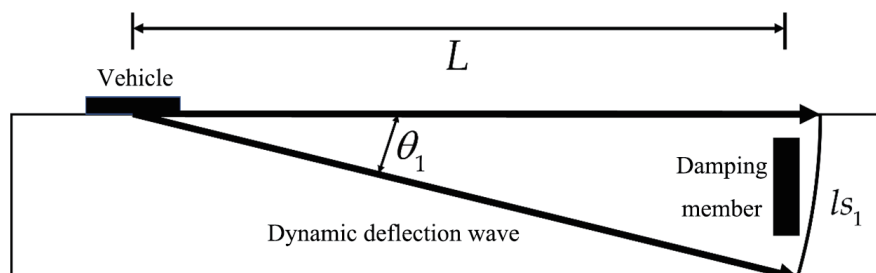


Fig. 2. Internal vibration propagation of bridge components under healthy condition.

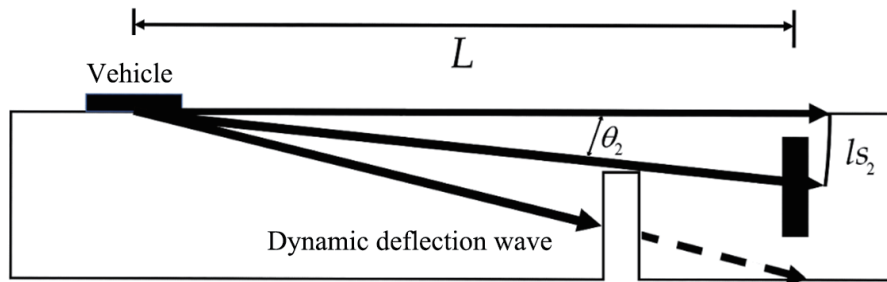


Fig. 3. Vibration propagation blocked by a bridge crack.

$$E_2 = \frac{\theta_2}{2\pi} E. \quad (3)$$

E_2 is the energy of the inner wave line ls_2 , and its energy per unit length ΔE_2 is

$$\Delta E_2 = \frac{\theta_2}{2\pi} E / ls_2. \quad (4)$$

Since the original direct wave line cannot be directly reached, ls_2 is the length of the wavefront that is hindered after the bridge cracks appear. Therefore, $E_1 < E_2$, and it can be proved that

$$\Delta E_1 = \Delta E_2 = \frac{E}{2\pi L}, \quad (5)$$

where L is the distance from the vehicle to the damper at this moment.

As shown in Fig. 4, the diffraction phenomenon will occur when the wave propagation inside the bridge is hindered by cracks. Therefore, different from the original propagation angle θ_1 , the diffraction makes the included angle θ_3 larger after the wave line passes through the crack. Since the wavefront length of the direct vibration has changed to ls_3 , the total energy of the direct vibration has not changed, so the energy per unit length becomes

$$\Delta E_2' = \frac{\theta_2}{2\pi} E / ls_3. \quad (6)$$

Since $ls_3 > ls_2$, $\Delta E_2' < \Delta E_2 = \Delta E_1$. Consequently, the energy per unit area is reduced due to diffraction as the wave passes through the crack. The dynamic deflection energy will be attenuated. When the propagation speed of the wave in the medium is constant, the frequency is inversely proportional to the wavelength. The vibration generated by the dynamic load has a lower frequency and a longer wavelength. In this situation, it is difficult for the damping member to receive the energy of a dynamic loading, so within a certain time window, the total energy near the crack will accumulate.

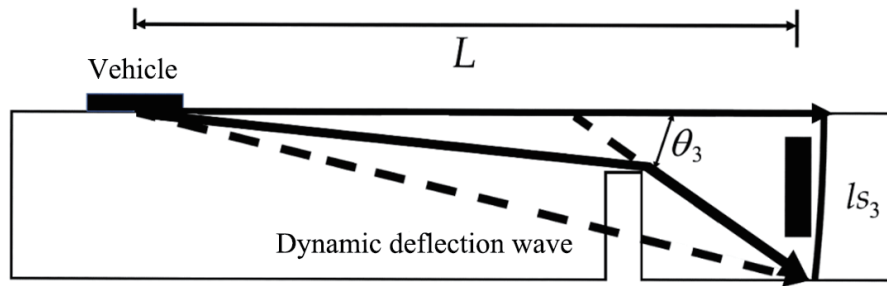


Fig. 4. Wave diffraction caused by a crack.

2.2 ESMD-based energy integral model construction

The ESMD method can adaptively decompose the original input signal into a series of IMF components and an adaptive global mean (AGM) curve. In ESMD decomposition, since the frequency and amplitude of each IMF component change with time, it is illogical to directly project energy information on fixed frequency points (or around fixed frequencies) quantitatively. The total energy of pulsation is not conserved, and the traditional spectral analysis methods (such as Fourier spectrum or Hilbert spectrum) based on the premise of constant energy cannot be applied to the ESMD results. Therefore, if the energy change feature is taken as a new research object, the j th IMF component result is regarded as an independent time scale function, which is

$$y_j(t) = A_j(t) \cos \theta_j(t). \quad (7)$$

A_j represents the amplitude curve of $y_j(t)$. In accordance with the total kinetic energy formula, the energy of each IMF component can be defined as

$$E_j(t) = \frac{1}{2} \sum_{i=1}^n A_j^2(t). \quad (8)$$

The sampling time is t and the number of samples is n . Since the original input signal can be obtained by superimposing all IMF components, the instantaneous energy of the original signal can also be obtained by adding the energy of all IMF components.

$$E(t) = \sum_{i=1}^m E(t) \quad (9)$$

$E(t)$ represents the instantaneous total energy of the original input signal, and m represents the number of IMFs.

Owing to the abnormality of bridge components, energy accumulation will occur near the location of the cracks. To explore the position and degree of bridge abnormality, in this paper, we propose to perform energy integration in a fixed time range for each reflection point on the lower surface of the bridge.

Figure 5 shows the layout of GB-SAR reflection points on the lower surface of the bridge. Reflection points RS1 to RS11 are laid out along the midspan of the bridge. By calculating the energy integral of each RS point, the energy integration value of the lower surface of the bridge for different positions of the same dynamic loading can be obtained, and then the position of the bridge abnormality can be judged. The energy integral EI of the instantaneous total energy can be defined as

$$EI = \int_{t_{\min}}^{t_{\max}} E(t) dt. \quad (10)$$

In Eq. (10), $E(t)$ represents the instantaneous energy function of the original input signal, and t represents the time window of integration.

Regarding how to define the time window T , in the traditional time–frequency analysis, if there is a certain damage and abnormality in the structure, the natural frequency of the structure will decrease. This can be reflected by monitoring the sudden drop in the instantaneous frequency of the structure.⁽¹⁹⁾ Therefore, the instantaneous frequency analysis using the ESMD method can judge the stability of the measured structure under dynamic loading by exploring the sudden change (decrease) in the instantaneous frequency of the main frequency of the signal.⁽¹⁹⁾ The time window of instantaneous frequency mutation obtained by the ESMD method can be regarded as the time range where the dynamic loading of the vehicle has the greatest effect on the RS points. In the time window, the vibration caused by the vehicle can fully propagate inside the bridge body, and a more typical result of instantaneous total energy integration can be obtained.

3. Experiment and Analysis of Results

In this study, the Beishatan Bridge is selected as the experimental bridge; it is one of the important components of the G6 Expressway in Beijing, China. The bridge is composed of left and right sub-bridges, and the known monitoring results show that the right sub-bridge has experienced a settlement of about 8 cm. To avoid further abnormality occurring in the right sub-bridge, it has been supported by jacks, as shown in Fig. 6.

An image by interferometric survey of structures (IBIS-S), a type of GB-SAR instrument, was applied to acquire the dynamic deflection of the two sub-bridges.⁽²¹⁾ For issues related to the instrument setup and the effect of atmospheric parameters on experimental results, please refer to Ref. 21. The IBIS-S instrument was located on one side of the bridge. The radar unit's angle of

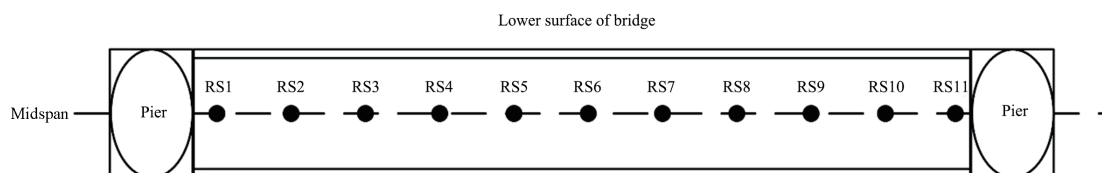


Fig. 5. Layout of reflection points on the lower surface of the bridge.



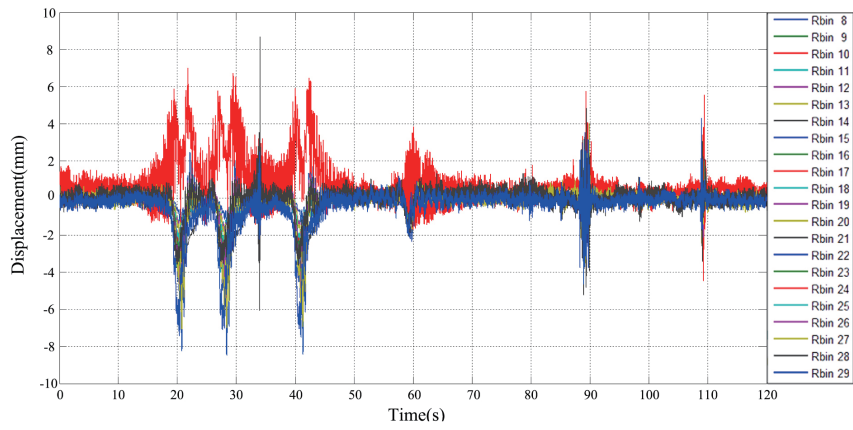
Fig. 6. (Color online) Beishatan Bridge in Beijing, China.

altitude was set as 26° . Each group contained 22 points with the sampling frequency of 113.33 Hz. The length of the signal was 120 s. In accordance with the workflow introduced in Fig. 1, in this study, we first adopt the ESMD-WSST high-frequency denoising method, which we have proposed before, to reduce the effect of noise on the monitored dynamic deflection results. The specific denoising principle and process are detailed in Ref. 20. Figure 7 shows the denoised dynamic deflection signals of the two sub-bridges. The signal after denoising still has a certain degree of noise residue, which is caused by the characteristics of ESMD decomposition, and there is still room for improvement in this direction.

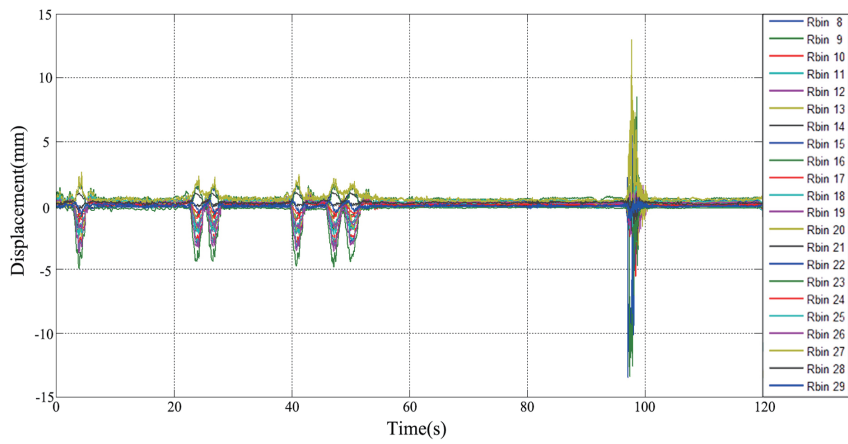
ESMD decomposition is then performed on the dynamic deflection data after noise reduction, and the time window T of energy integration is obtained by calculating the instantaneous frequency.

To obtain more typical results, the reflection point with the largest change in the dynamic deflection of both left and right sub-bridges is selected as a reference. For the left sub-bridge, point Rbin24 (maximum deflection 8.63 mm) is chosen, and for the right sub-bridge, point Rbin22 (maximum deflection 13.17 mm) is chosen. Figure 8 shows the instantaneous frequency change of the reflection point Rbin24 on the left sub-bridge. The red square in the figure shows that the instantaneous frequency decreases significantly in the interval from 14 to 67 s. Figure 9 shows the instantaneous frequency change of the reflection point Rbin22 on the right sub-bridge. The red square in the figure shows that the instantaneous frequency decreases significantly in the interval from 18 to 62 s. Widening the time window can reduce the interference of edge effects, so the energy integration time of the left sub-bridge was set as $T_1 = [10, 71]$ and that of the right sub-bridge was set as $T_1 = [18, 62]$.

In accordance with Eq. (10), T_1 and T_2 are used to integrate the energy of all reflection points on the left and right sub-bridges, respectively, and the integration results are shown in Tables 1 and 2. It can be seen from Table 1 that the energy change of the left sub-bridge is relatively gentle, and the point Rbin24 has obtained the largest energy integral of 140.9261 at a horizontal distance of 16.6 m. Table 2 shows that the energy of the right sub-bridge fluctuates considerably, and there are two reflection points Rbin16 and Rbin22 with large energy integral mutations,



(a)



(b)

Fig. 7. (Color online) Overview of dynamic deflection after ESMD-WSST denoising. Denoised dynamic deflection of (a) left sub- and (b) right sub-bridges.

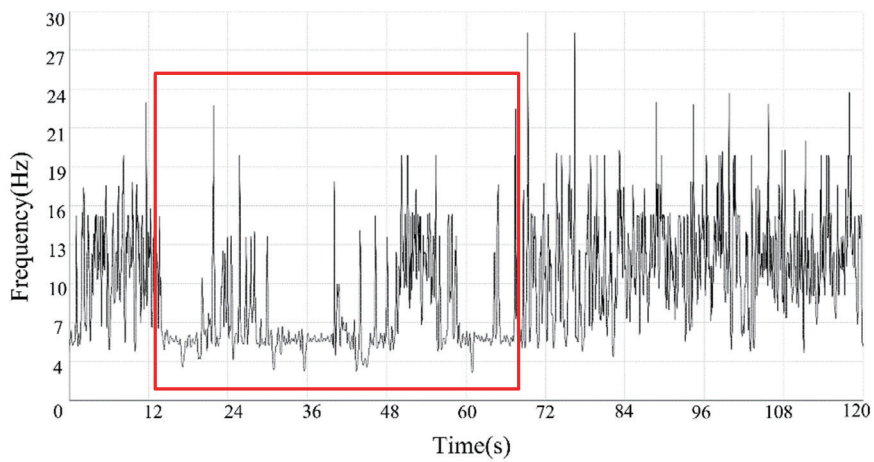


Fig. 8. (Color online) Instantaneous frequency change of main vibration mode of left sub-bridge.

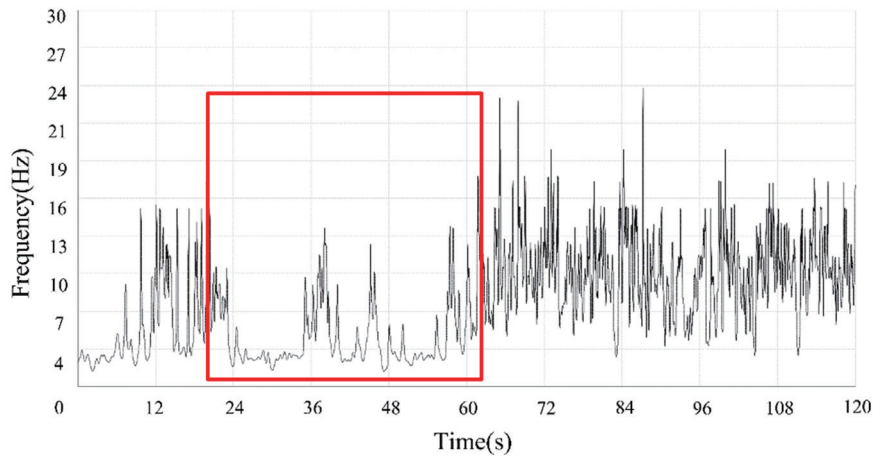


Fig. 9. (Color online) Instantaneous frequency change of main vibration mode of right sub-bridge.

Table 1

Energy integration results of all reflection points of the left sub-bridge.

Reflection points	Rbin8	Rbin9	Rbin10	Rbin11	Rbin12	Rbin13	Rbin14	Rbin15	Rbin16	Rbin17	Rbin18
Horizontal distance (m)	1.6	3.3	4.6	5.6	6.6	7.5	8.4	9.3	10.1	10.9	11.8
Energy integration	2.7689	10.3612	8.1392	10.5119	14.1569	17.3247	15.6212	28.2039	22.3829	23.3708	19.9832
Reflection points	Rbin19	Rbin20	Rbin21	Rbin22	Rbin23	Rbin24	Rbin25	Rbin26	Rbin27	Rbin28	Rbin29
Horizontal distance (m)	12.6	13.4	14.2	15.0	15.8	16.6	17.3	18.1	18.9	19.7	20.5
Energy integration	28.3573	26.8473	21.0767	25.5452	45.3735	140.9261	46.7376	21.3127	15.621	22.2915	22.7781

Table 2

Energy integration results of all reflection points of the right sub-bridge.

Reflection points	Rbin8	Rbin9	Rbin10	Rbin11	Rbin12	Rbin13	Rbin14	Rbin15	Rbin16	Rbin17	Rbin18
Horizontal distance (m)	1.6	3.3	4.6	5.6	6.6	7.5	8.4	9.3	10.1	10.9	11.8
Energy integration	5.3762	5.0415	5.0442	7.8028	16.9166	20.0845	16.2250	28.9991	117.9819	25.1440	21.4363
Reflection points	Rbin19	Rbin20	Rbin21	Rbin22	Rbin23	Rbin24	Rbin25	Rbin26	Rbin27	Rbin28	Rbin29
Horizontal distance (m)	12.6	13.4	14.2	15.0	15.8	16.6	17.3	18.1	18.9	19.7	20.5
Energy integration	22.3068	20.2216	16.8124	120.8181	6.4011	12.0530	11.7267	19.9687	26.0411	11.6862	5.1193

which are located at horizontal distances of 10.1 and 15.0 m, respectively. Rbin16 has the energy integration of 117.9819, and Rbin22 has the largest energy integration of 120.8181. Since the right sub-bridge has an accurate location reference for the cracks, the reflection point Rbin22 with the largest energy integral result is located near the reinforcement jack of the right bridge, at a horizontal distance of about 15.2 m from the pier column. The results preliminarily prove the effectiveness of the proposed method for bridge abnormality detection.

To further explore whether the remaining two reflection points with large integrals are accurately located at the position of the bridge abnormality, the experimental results were compared with the 3D laser point cloud model in the same period. Figure 10 shows the digital surface model (DSM) of the undersurface of Beishatan Bridge constructed from point cloud. At 16.2 m on the left sub-bridge, there is a settlement strip with a length of 7.8 cm. At 14.9 m on the right sub-bridge, there is a settlement strip with a length of 9.7 cm. At the same time, at 16.8 m on the right sub-bridge, there is also a relatively clear settlement, as shown in the black block. These settlement areas are perfectly consistent with the results obtained in this study (16.6 m for the left sub-bridge and 10.1 and 15.0 m for the right sub-bridge), which confirms that the ESMD-based energy integral model proposed in this paper can accurately detect the position and trend of the bridge abnormality.

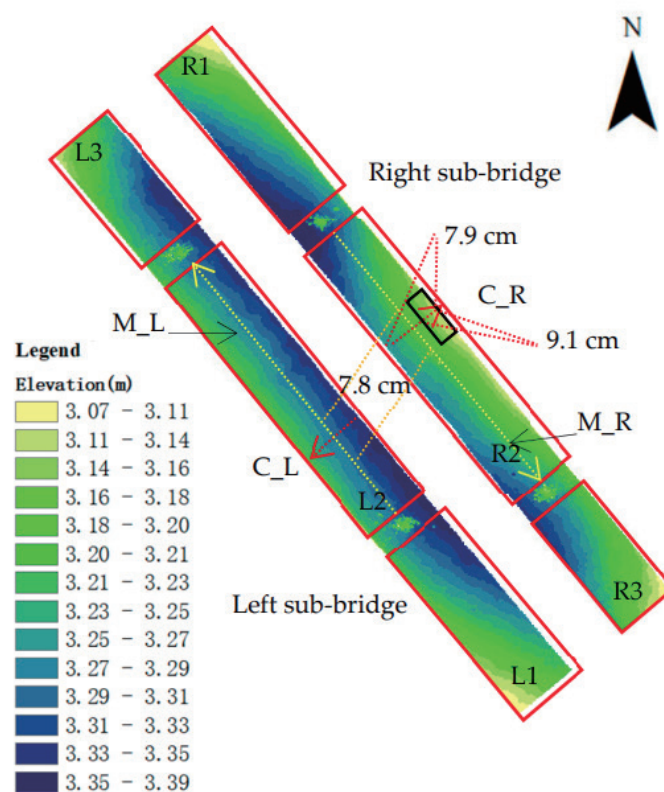


Fig. 10. (Color online) DSM model constructed from point cloud of Beishatan Bridge.

4. Conclusion

With the advantages of noncontact measurement, high speed, and high precision, GB-SAR is widely used in bridge dynamic deflection monitoring. The TFA method of energy analysis is used to identify the abnormality of bridge dynamic deflection. As one of the emerging TFA methods, the ESMD method can adaptively deal with bridge dynamic deflection and perform energy analysis. To improve the accuracy of energy analysis results and quantitatively analyze the abnormality of bridges, in this paper, we propose an ESMD-based energy integral model for bridge abnormality detection. More specifically, the results presented in this paper clearly highlight the following.

- (1) After ESMD decomposition, the total kinetic energy formula can be used to obtain the relationship between the dynamic deflection signal energy and time, which avoids the problem of projecting time-varying energy on a fixed frequency band by the energy spectrum method and improves the accuracy of energy analysis results.
- (2) Through the calculation of instantaneous frequency, the main vibration mode of the original signal and the typical time window of dynamic loading are obtained adaptively. It can make the result of the subsequent energy integration more readable and can more accurately identify the position of the bridge variation.
- (3) Referring to the relationship between the bridge variation and the energy accumulation, an ESMD-based instantaneous total energy integration method is proposed, which avoids the empirical judgment of the traditional ESMD method in energy analysis. The position and trend of the bridge variation can be detected from the quantitative energy integration results.
- (4) The experimental results are compared with the previously known bridge crack positions to verify the effectiveness of the algorithm. Further comparison with the DSM of the same period verifies that the ESMD-based energy integral model proposed in this paper can accurately identify the position and trend of bridge abnormalities.

Owing to the residual noise in the IMF components obtained from ESMD decomposition, there is still room for improvement in the ESMD-WSST denoising method used in this paper. Concerning the applicability of the method described in this paper, the energy integral model is suitable for structures with damping elements, such as bridges, and it is difficult to detect the abnormalities of other types of structure by this method.

Acknowledgments

This research was funded by the Ministry of Science and Technology of the People's Republic of China, grant number 2018YFE0206100; the National Natural Science Foundation of China, grant numbers 41871367 and 42201488; the Joint Project of Beijing Municipal Commission of Education and Beijing Natural Science Foundation, grant number KZ202210016022; the Pyramid Talent Training Project of Beijing University of Civil Engineering and Architecture, grant number JDJQ20220804; the Fundamental Research Funds for Beijing Universities, grant number X20150; the Young Teachers Research Capability Enhancement Program of Beijing University of Civil Engineering and Architecture, grant number X22019; and the BUCEA Postgraduate Innovation Project.

References

- 1 E. Ntsios, C. Papadimitriou, P. Panetsos, G. Karaiskos, K. Perros, and P. C. Perdikaris: *Bull. Earthquake Eng.* **7** (2009) 469. <https://doi.org/10.1007/s10518-008-9067-4>
- 2 H. H. Kai, W. H. Marvin, and P. J. Barr: *J. Bridge Eng.* **11** (2006) 707. [https://doi.org/10.1061/\(ASCE\)1084-0702\(2006\)11:6\(707\)](https://doi.org/10.1061/(ASCE)1084-0702(2006)11:6(707))
- 3 G. Carmelo and B. Giulia: *Struct. Infrastruct. Eng.* **6** (2010) 521. <https://doi.org/10.1080/15732470903068557>
- 4 S. Qian and C. Dapang: *IEEE Signal Process. Mag.* **16** (1999) 52. <https://doi.org/10.1109/79.752051>
- 5 R. G. Baraniuk and D. L. Jones: *IEEE Trans. Signal Process.* **41** (1993) 1589. <https://doi.org/10.1109/78.212733>
- 6 R. N. Bracewell: *The Fourier Transform and Its Applications* (McGraw-Hill, New York, 1986) pp. 267–272.
- 7 H. J. Nussbaumer: *Fast Fourier Transform* (Springer, Berlin Heidelberg, 1982) pp. 80–111. https://doi.org/10.1007/978-3-642-81897-4_4
- 8 D. Griffin and J. Lim: *IEEE Trans. Signal Process.* **32** (1984) 236. <https://doi.org/10.1109/TASSP.1984.1164317>
- 9 J. B. Allen and L. R. Rabiner: *Proc. IEEE* **65** (1977) 1558–1564. <https://doi.org/10.1109/PROC.1977.10770>
- 10 N. Hess-Nielsen and M. V. Wickerhauser: *Proc. IEEE* **84** (1996) 523–540. <https://doi.org/10.1109/5.488698>
- 11 P. Kumar and E. Fofoula-Georgiou: *Rev. Geophys.* **35** (1997) 385. <https://doi.org/10.1029/97RG00427>
- 12 N. E. Huang, Z. Shen, S. R. Long, M. C. Wu, H. H. Shih, Q. Zheng, N. Yen, C. C. Tung, and H. H. Liu: *Proc. Royal Society of London. A* **454** (1998) 903–995. <https://doi.org/10.1098/rspa.1998.0193>
- 13 M. Jiang, X. Liu, H. Wang, and Y. Huang: *Sens. Mater.* **32** (2020) 4471. <https://doi.org/10.18494/SAM.2020.3126>
- 14 J. L. Wang and Z. J. Li: *Climate Change Res. Lett.* **3** (2014) 4. <https://doi.org/10.12677/CCRL.2014.31001>
- 15 J. L. Wang and Z. J. Li: *Adv. Adapt. Data Anal.* **5** (2013) 1350015. <https://doi.org/10.1142/S1793536913500155>
- 16 J. Wang and X. Fang: *Int. J. Geomech.* **6** (2015) 481. <https://doi.org/10.4236/ijg.2015.65038>
- 17 J. N. Yang, Y. Lei, S. Pan, and N. Huang: *Earthquake Eng. Struct. Dyn.* **32** (2003) 1443. <https://doi.org/10.1002/eqe.287>
- 18 N. Roveri and A. Carcaterra: *Mech. Syst. Signal Process.* **28** (2012) 128. <https://doi.org/10.1016/j.ymsp.2011.06.018>
- 19 X. Liu, Y. Tang, Z. Lu, H. Huang, X. Tong, and J. Ma: *Measurement* **120** (2018) 34. <https://doi.org/10.1016/j.measurement.2018.01.038>
- 20 S. Rödelsperger, G. Läufer, C. Gerstenecker, and M. Becker: *J. Appl. Geod.* **4** (2010) 41. <https://doi.org/10.1515/jag.2010.005>
- 21 X. Liu, S. Zhao, and R. Wang: *Electronics* **12** (2023) 54. <https://doi.org/10.3390/electronics12010054>

